CHARACTERISTIC BEHAVIORS ON ATOMIC STRUCTURE AND ELECTRONIC STATE OF Fe-B GLASSY ALLOYS

Supplement to Sci. Rep. RITU, A, March, 1980

CHARACTERISTIC BEHAVIORS ON ATOMIC STRUCTURE AND ELECTRONIC STATE OF Fe-B GLASSY ALLOYS

K.Suzuki, F.Itoh, M.Misawa, M.Matsuura*, T.Fukunaga and K.Ikeno

The Research Institute for Iron, Steel and Other Metals, Tohoku University, Sendai-980, Japan

*Miyagi Technical College, Natori, Miyagi-981-12, Japan

ABSTRACT

Fe-B glassy alloys with 12-25 at%B content were prepared by a single roll in controlled ambient gas atmospheres. The surface profile of glassy alloy ribbons was examined using an optical microscope. The density, X-ray interference function, XPS and γ-ray Compton profile of Fe-B glassy alloys were measured as a function of B content at room temperature. Characteristic behaviors on the atomic structure and electronic state of Fe-B glassy alloys have been discussed in terms of the correlation between various physical properties measured in this study.

INTRODUCTION

A lot of attention has been focused on Fe-B alloys in the glassy state quenched from the molten state, because Fe-B glassy alloys are not only one of the most successful materials for the application of energy-saving electronic devices[1] but also indicate remarkably characteristic composition dependences in various physical properties such as crystallization process[2,3], density[4], coordination number[4,5], magnetic moment [6], Curie temperature[2], internal field distribution[7] and so on.

There are, however, difficult technical problems concerning non-uniformity in the surface flatness of melt-quenched glassy alloy ribbons, which is essentially important for the device application where a large number of thin ribbons are heaped so as to obtain a high volume efficiency. In this study, we report the effect of ambient gases on the optical microscope scale surface profile of Fe-B-Si glassy alloy ribbons fabricated by a single roll melt-spinning technique.

Physical properties of glassy alloys are inherently rather structure-sensitive than those of crystalline alloys, because the freedom of atomic

arrangement is quite large in the glassy state and furthermore the metastable glassy structure always exists in the relaxation process. Therefore this study is aimed at examining the correlation between the atomic structure and electronic state in Fe-B glassy alloys. The atomic structure particularly Fe-Fe partial pair correlation in Fe-B glassy alloys was selectively observed as a function of B content by X-ray diffraction, since Fe-B and B-B partial pair correlations contribute little to the measured total pair correlation function because of a negligibly small scattering factor of B atom compared with that of Fe atom.

The electronic energy spectrum and wave function of Fe-B glassy alloys were directly measured using XPS and γ-ray Compton scattering technique, respectively. The both techniques are very powerful to probe the electronic structure in disordered materials as well as in ordered crystalline materials. The formation of chemical bonding and charge transfer between Fe and B atoms in Fe-B glassy alloys are discussed based on experimental observations in this study.

SURFACE PROFILE OF MELT-QUENCHED RIBBONS

A schematic diagram and photograph of the apparatus used to fabricate Fe-12at%B-10at%Si glassy alloy ribbons in various ambient gas-atmospheres are shown in Fig. 1. After melting a master alloy in a quartz cell by r. f heating in the vacuum chamber, the quartz cell is shifted down to just above a spinning roll and then the melt is ejected onto the surface of the roll. Continuous alloy ribbons thus fabricated fly into the receiving tube attached to the vacuum chamber.

In order to examine the ambient gas effect, some conditions of fabrication such as cooling rate, pressure for ejecting and ambient gas pressure were maintained, i.e. the surface velocity of a spinning copper roll was 62.8 m/s, orifice diameter 0.8 mm, the pressure of Ar for ejecting molten metal 3×10^4 Pa(0.3 atm) and the ambient gas pressure 6.1×10^4 Pa(0.6 atm). He, N_2, Ar and Air were used as ambient gases in this study.

Fig. 2 shows profiles of the surface contacing to the roll of the glassy alloy ribbons fabricated in Ar, He and vacua(0.16 Pa = 1.2×10^{-3} Torr). The casting direction from melt is parallel to the direction of long streaks in the photographs.

On the surface of ribbons fabricated in Ar and the air, there are many and large scratches due to gas bubbles injected along melt-roll interface. On the other hand, though small and rare scratches due to gas bubbles still remain on the surface of ribbons fabricated in He, the number of scratches is remarkably small compared with those in Ar or the air. As a matter of course, such scratches due to gas bubbles are absent on the ribbon surface fabricated in vacua. In particular, edge parts of the bottom surface of ribbons fabricated in He and vacua are very sharp and smooth, but a little amount of He gas bubbles seems to be injected along melt-roll interface near edge.

The feature of surface roughness of Fe-12at%B-10at%Si glassy alloy was examined by a pilofilometer. The measurement of profile curves were carried out across the width of ribbon surfaces with both free and bottom surfaces. The profile curve of the bottom surface of the ribbon fabricated in Ar shows more frequent and deeper notches caused by hollows compared

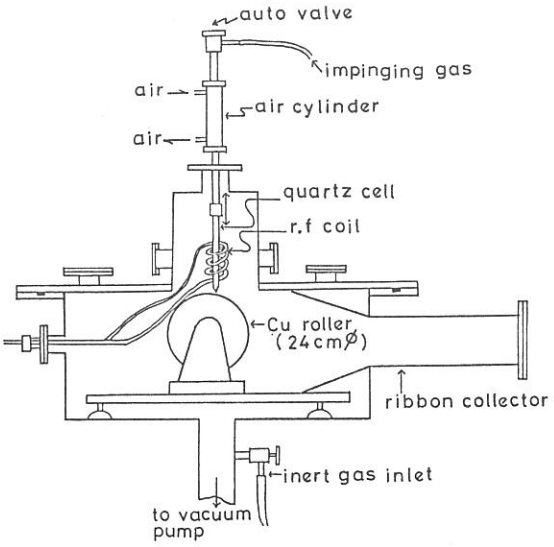

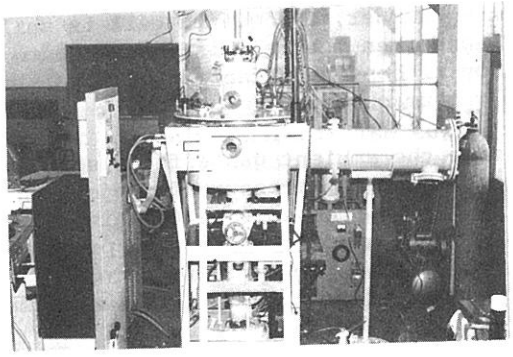

Fig. 1 Schematic diagram and photograph of the apparatus used to prepare glassy alloy ribbons by melt-spinning technique in various ambient gas atmospheres.

with those of He and vacua. The profile curve of the free surface of the ribbon fabricated in Ar has many and extremely large ups and downs, while the free surfaces of the ribbons fabricated in He and vacua have high qualities with even and flat surfaces.

Microphotgraphs of the longitudinal cross-section of multi-layered Fe-12at%B-10at%Si glassy alloy ribbons fabricated in Ar, He and vacua are shown in Fig. 3. Dark sections sandwiched between ribbons in each photograph indicate the adhesive agent used to heap ribbons. The bottom surface of ribbons fabricated in He and vacua shown in Fig. 3(b) and (c) is flat like the upper free surface. Uniformity of the thickness of the ribbons fabricated in He and vacua is excellent. Only small amd rare hollows due to gas bubbles indicated in Fig. 3(b) by an arrow can be

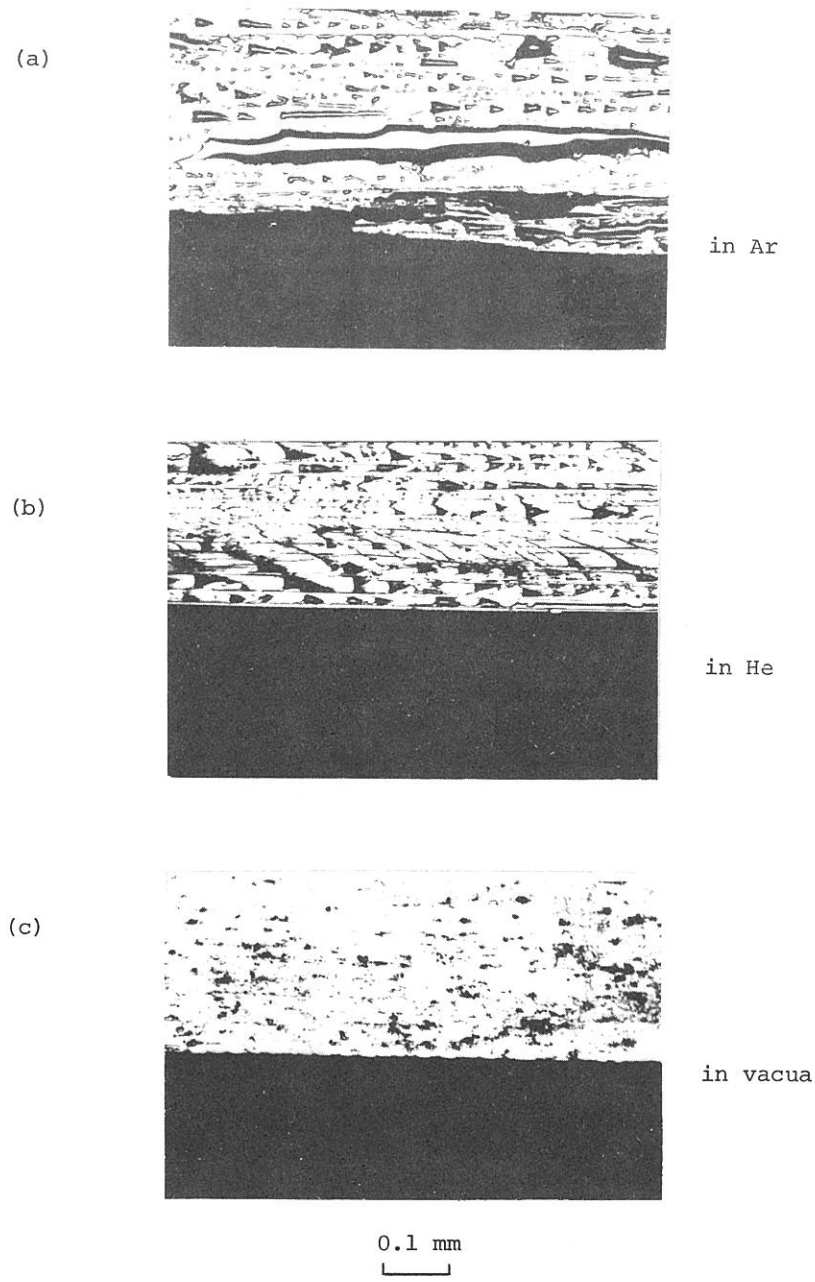

Fig. 2 Surface profiles near edge of Fe-12at%B-10at%Si glassy alloy ribbons fabricated using a single roll technique in (a) Ar, (b) He and (c) vacua.

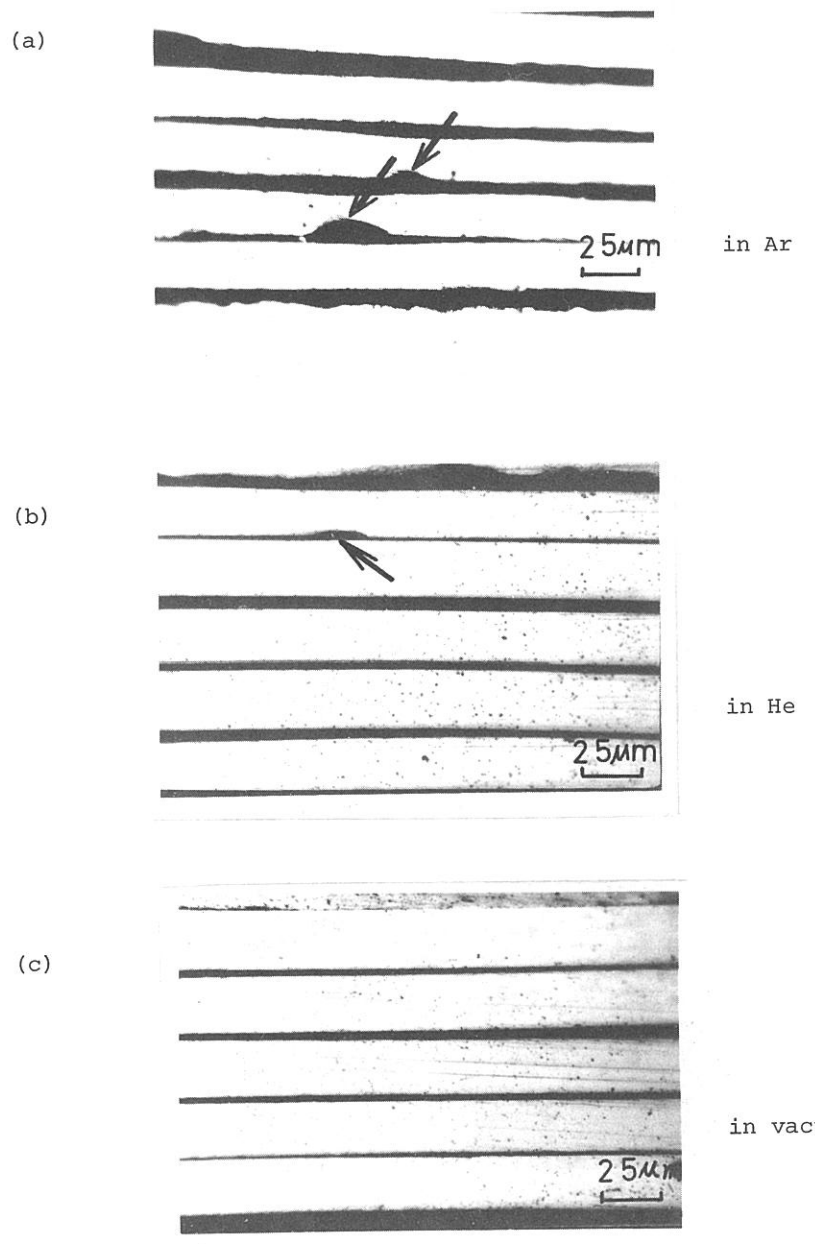

Fig. 3 Longitudinal cross-sections of multi-layered Fe-12at%B-10at%Si glassy alloy ribbons fabricated using a single roll technique in (a) Ar, (b) He and (c) vacua. Dark areas between ribbons are adhesive agent used to heap ribbons. The bottom of ribbon is the surface contacting the roll. Arrows in photographs indicate hollows due to gas bubbles.

observed in the longitudinal cross-section of robbons fabricated in He. However, the longitudinal cross-section of the ribbon fabricated in Ar is significantly different from those fabricated in He and vacua. There are large and many hollows due to gas bubbles in the bottom surface and occasionally their depth attains almost a half of the thickness of ribbons. Therefore, multi-layered glassy alloy ribbons fabricated in Ar have low volume efficiency. The same facts can be observed in case of the ribbons fabricated in the air and N_2.

When a roll is rotated at high spinning rate in a gas, a thin gas boundary layer is formed on the surface of spinning roll because of the frictional interaction between the roll surface and ambient gas[8]. This thin gas boundary layer of which velocity is essentially same to the roll surface velocity must be injected along melt-roll interface and this brings about scratches or hollows due to gas bubbles on the bottom surface of a ribbon contacting to roll surface.

The pressure of a thin gas boundary layer is proportional to the den =sity and the pressure of an ambient gas. Therefore, as suggested by Liebermann[8] and Anthony and Cline[9], low pressure of ambient gas and/ or low atomic weight ambient gas such as He and H_2 facilitate the fabrication of smooth ribbons without serrated edges. We found that the surface profile of glassy alloy ribbons has been affected seriously by ambient gas atmospheres.

SHORT-RANGE ATOMIC STRUCTURE

The measurement of the interference function S(Q) of Fe-B glassy alloys was carried out by means of conventional X-ray diffraction. MoKα radiation impinged on the thin ribbons and the scattered intensity of transmitted MoKα radiation was counted, after being monochromtized by pyrolytic graphite, over a scattering angle range from 2 to 120 deg using a step scan with an interval of 0.1 deg. Corrections for background, absorption, anomalous scattering, Compton scattering and multiple scattering were applied for deducing S(Q) from the measured intensity.

The experimental S(Q) of Fe-B glassy alloys is shown as a function of B content in Fig. 4. The composition dependence of the first peak height in S(Q) indicates a steep increase including an inflection point near 16-18 at% B content and its FWHM varies in the opposite way showing steep decrease, when B content in the alloy is increased. The famous shoulder on high Q side of the second peak in S(Q) becomes less pronounced with increasing B content.

Fig. 5 shows the total pair correlation function g(r) of Fe-B glassy alloys obtained as Fourier transform of S(Q) truncated at Q=150 nm^{-1}. As shown in Fig. 6, the first peak position in RDF is linearly increased with a quite small slope over a low B content region and then reaches a saturated value at approaching 22 at% B, as B atoms are added. The value of the first peak position is extrapolated toward a value obtained for an evaporated Fe film by Ichikawa[10]. The same trend can be found in case of Fe-P glassy alloys studied by Logan[11].

The present result indicates a sharp contrast against the experimental observation by Waseda and Chen[5], who have found that the second peak shoulder in S(Q) increases with B content and an extraordinarily deformed

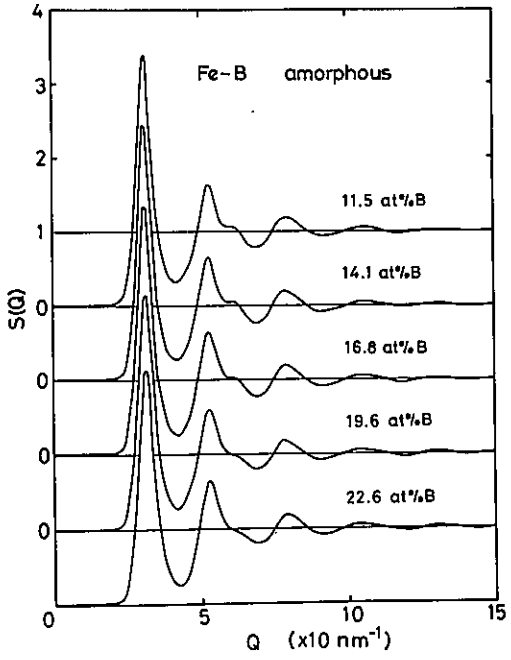

Fig. 4 Interference functions S(Q) of Fe-B glassy alloys.

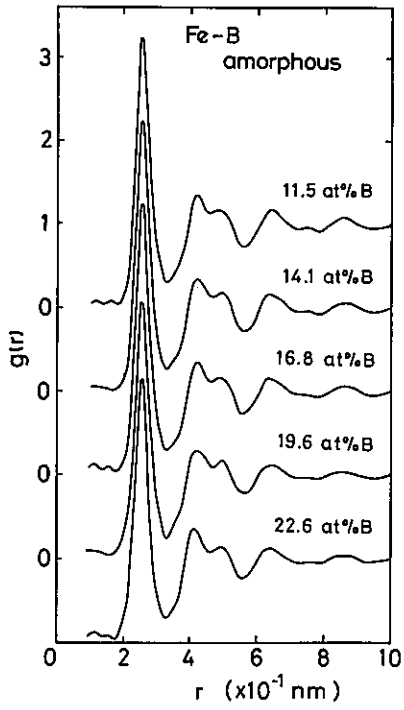

Fig. 5 Total pair correlation functions g(r) of Fe-B glassy alloys.

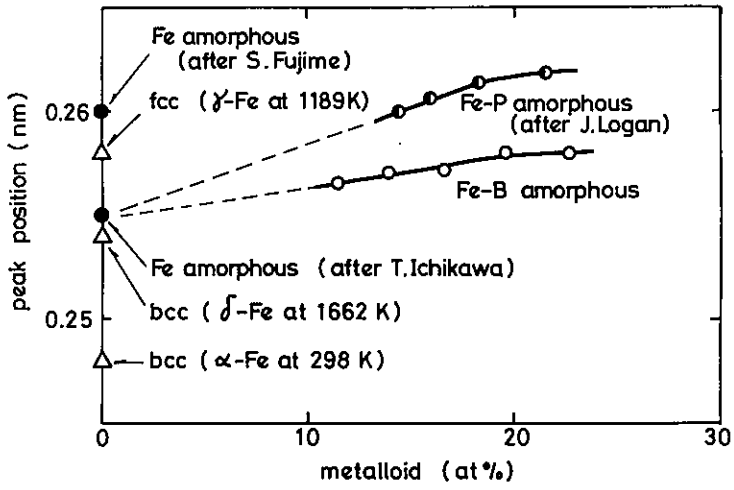

Fig. 6 First peak positions in RDF of Fe-B glassy alloys, Fe-P glassy alloys[11] and evaporated Fe film[10, 13].

relative height appears in the second peak splitting in g(r) of Fe-16at%B glassy alloy. Currently Cowlam et al have measured S(Q) of isotopically enriched Fe-17at%^{11}B glassy alloy by neutron diffraction[12], of which Fourier transform yields g(r) rather similar with our result. For comparison, the S(Q) and g(r) of Fe-B glassy alloys obtained by them are shown in Figs. 7 and 8.

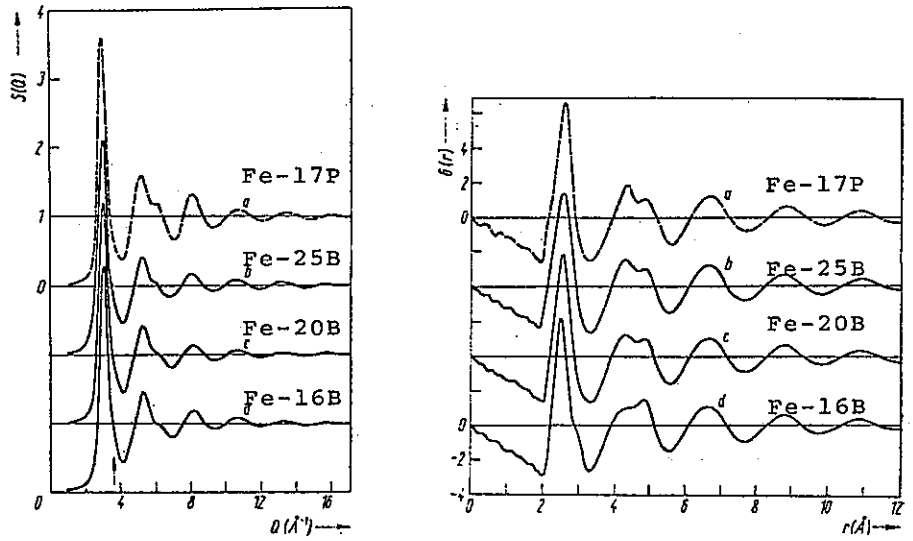

Fig. 7 X-ray interference functions S(Q) and reduced radial distribution functions G(r) of Fe-B glassy alloys obtained by Waseda and Chen[5]

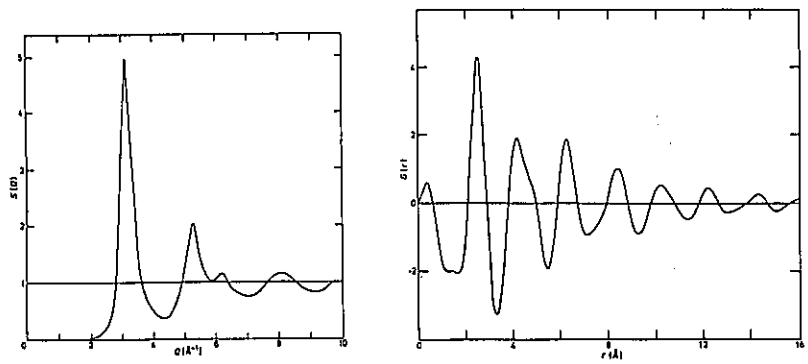

Fig. 8 Neutron interference function S(Q) and reduced radial distribution function G(r) of isotope-enriched Fe-17at%^{11}B glassy alloy obtained by Cowlam et al[12].

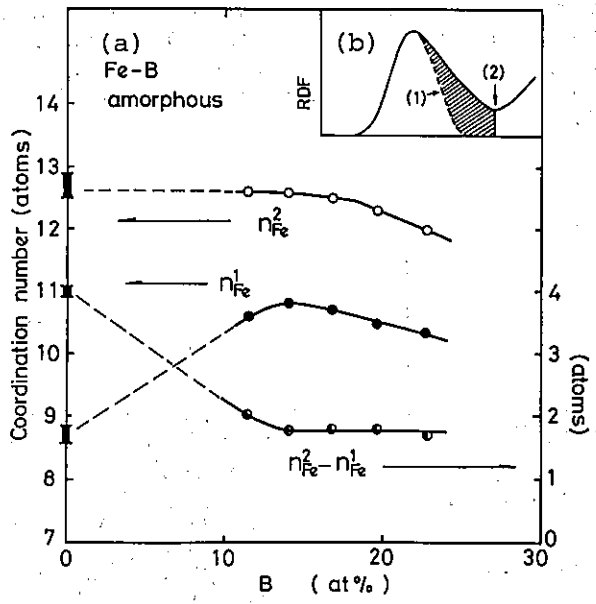

Fig. 9 Nearest neighbor coordination numbers in Fe-B glassy alloys, (a) composition dependence of nearest neighbor coordination numbers and (b) definition of areas under the first peak in RDF.

Fig. 9(a) shows composition dependence of the nearest neighbor coordination number in Fe-B glassy alloys, which is usually calculated from the area of the first peak in RDF. There have been known several ways to define the peak area so far. The area calculated by integrating the region under the first peak in RDF up to the first minimum position, as shown by (2) in Fig. 9(b), is the most commonly accepted definition of the nearest neighbor coordination number(n^2_{Fe}). This definition provides the largest value of the coordination number among several definitions. The smallest value of the coordination number (n^1_{Fe}) is obtained by defining the symmetrical peak around the first peak maximum in RDF, as shown by (1) in Fig. 9(b).

Values of n^2_{Fe} keep a constant value of 12.6±0.1 Fe atoms up to 17 at %B and show a monotonic drop beyond 18 at%B. By extrapolating towards no B content, the value of n^2_{Fe} for pure Fe amorphous film[10] is found to approach a value corresponding to the state of the packing fraction η=0.65 -0.67 and atomic diameter σ=0.25 nm. On the other hand, the composition dependence of n^1_{Fe} shows a broad maximum peak near the composition of 14-16 at%B, where a bend happens in $n^2_{Fe}-n^1_{Fe}$ curve.

Fig. 9(a) shows that Fe atoms transfer from a hatched area in RDF as shown in Fig. 9(b) to the symmetrical first peak region , when B content is increased. Such a behavior can be directly recognized by comparing the first peak profiles in RDF of pure Fe amorphous film[10] and Fe-22at%B glassy alloy, as shown in Fig. 10. A drastic modification in the topological arrangement of Fe atoms in Fe-B glassy alloys may appear at a composition range from 14 to 16 at%B, beyond which the value of n^1_{Fe} and n^2_{Fe} are continually decreased and therefore the value of $n^2_{Fe}-n^1_{Fe}$, i.e. the number of Fe atoms existing at the hatched area in RDF indicates little variation.

Such a feature in the composition dependence of atomic arrangement in Fe-B glassy alloys can be anticipated from the behavior of average density of the alloys, too. As shown in Fig. 11, the density of Fe-B glassy alloys does not vary appreciably in a composition range below 14-16 at%B, whereas a rapid decrease appears in the density curve for the alloys with higher B content. If B atoms are assumed to occupy interstitial holes in the dense random packing structure of Fe atoms which slightly expands due to B atom addition, the density of Fe-B glassy alloys can be calculated as a function of B content and indicates a very small increase with increasing B content, as shown by a hatched area in Fig. 11. This simple model can explain the composition variation in the density of Fe-B glassy alloys with low B content, but the rapid decrease in the density in higher B content region suggests that a large perturbation occurs in Fe atom arrangement in the glassy state by adding B atoms beyond 14-16 at%B.

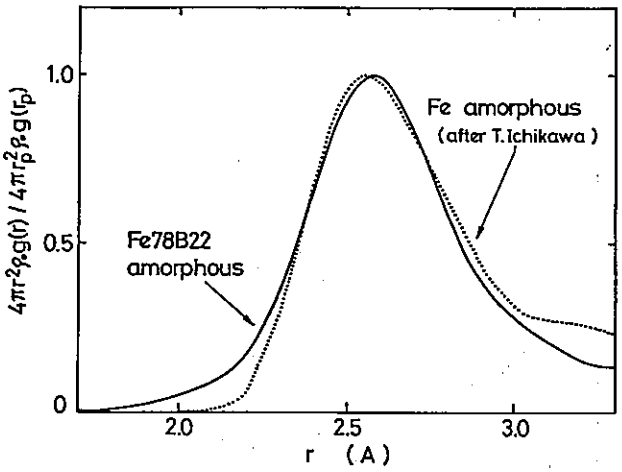

Fig. 10 Comparison of first peak profile in RDF between Fe amorphous film[10] and Fe-22at%B glassy alloy.

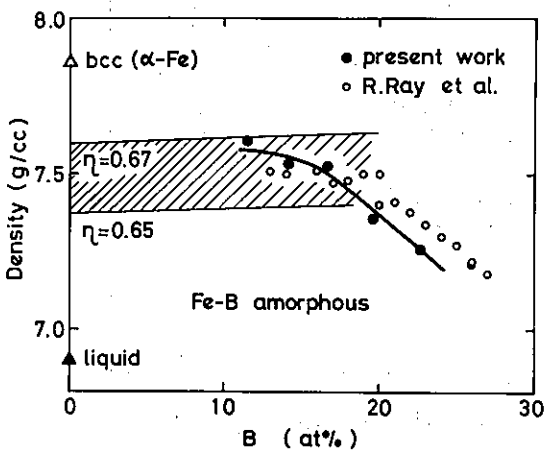

Fig. 11 Compositional variation in average density of Fe-B glassy alloys.

X-RAY PHOTOEMISSION SPECTROSCOPY

The X-ray photoemission spectroscopy(XPS) measurement of Fe-B glassy alloys was carried out as a function of B content. The alloys used were prepared in Ar gas atmosphere so as to prevent the surface oxidation of resultant alloys during vitrification from the molten state.

The resolution for XPS(AlKα excitation) was 1.05 eV which was determined from the FWHM of Au $4f_{7/2}$ level. To remove the surface contamination of as-prepared Fe-B glassy alloys, Ar ion sputtering was carried out for 10 minutes. No concentration change in the alloys due to the sputtering was confirmed by estimating the intensity ratio of the spectrum for Fe 3p level to that for B 1s level. The binding energy(B.E.) calibration was carried out by measuring Fe 3s(92.9 eV) and Fe 3p(54.0 eV) levels of pure iron in each XPS measurement.

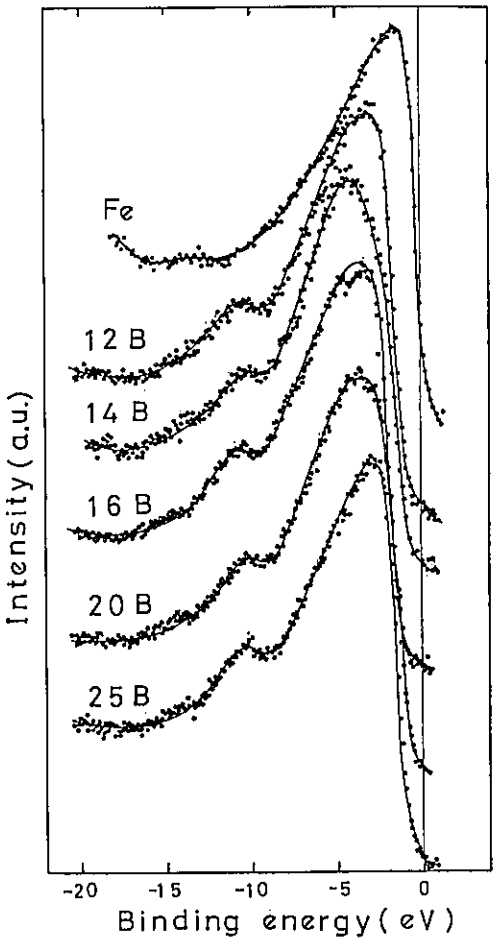

Fig. 12 Valence band spectra of Fe-B glassy alloys and pure Fe crystal.

The profiles of the valence band spectra(VBS) for Fe-B glassy alloys are shown as a function of B content together with that for pure Fe crystal in Fig. 12. One of the features of VBS for Fe-B glassy alloys, which obviously differs from that for pure Fe crystal, is that a small hump appears at a lower energy side of the maximum peak associated with Fe 3d band. The intensity and B.E. of this hump do not change significantly with B content. Another feature of the VBS for Fe-B glassy alloys is that the peak position of Fe 3d band shifts toward the energy region lower than that for pure Fe crystal. In Fig. 13 the peak shift of Fe 3d band is plotted against B content. This plot indicates a pronounced maximum at about 14 at%B.

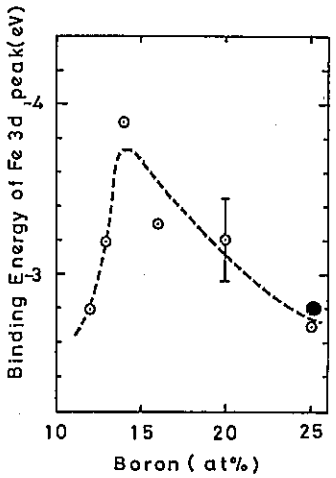

Fig. 13 Peak shift of Fe 3d band of Fe-B glassy alloys with B content. Solid circle is the value for crystalline Fe_3B.

In order to compare XPS between glassy and crystalline state, Fe-25 at%B alloy was chosen, because Fe-25at%B glassy alloy made polymorphous crystallization to a metastable and homogeneous Fe_3B phase at about 650 K. Crystalline Fe_3B was prepared by annealing Fe-25at%B glassy alloy at 820 K for one hour in vacua(5×10^{-8} Torr). The XPS for crystalline Fe_3B exhibited no significant change in Fe 3s and Fe 3p levels and Fe 3d band including the hump from those for Fe-25at%B glassy alloy.

We conclude that the origin of the hump appearing at lower energy side of Fe 3d band comes out from a bonding state newly created between B 2p and Fe3d electrons in Fe-B glassy alloys. The appearence of such a bondong state at lower energy region of 3d band has been suggested in the case of transition metal based alloys containing non-transition elements by Terakura and Kanamori[14] and transition metal-hydrogen alloys by Tanaka[15] and Itoh et al[16].

The absence of any appreciable variation in the intensity and B.E. of the hump with B content can be understood in terms of the appearence of the bonding state between B and Fe atoms, if it is supposed that B atoms occupy interstitial-like sites below some critical B content, probably below 14 at%B , and excess B atoms occupy substitutional-like sites in higher B content[7]. Namely, the bonding states may be formed between Fe and interstitial-like B atoms, because the interatomic distances between

Fe and interstitial-like B atoms are shorter than those between Fe and substitutional-like B atoms. Therefore, the intensity and B.E. of the hump are saturated in Fe-B glassy alloys examined in this study.

Substitutional-like B atoms in Fe-B glassy alloys may deform the profile of Fe 3d band over the concentration range more than 14 at%B. In fact, Fig.12 shows that the observed profile of Fe 3d band for Fe-B glassy alloys is scraped off around high energy side of peak and this lack is gradually recovered according to the increase of B content. Based on these observations, the electronic structure of Fe 3d band in Fe-B glassy alloys can be regarded to be quite far from a conventional rigid band model.

The absence of any striking difference of XPS between Fe-25at%B glassy alloy and crystalline Fe_3B strongly supports that the both phases have a close similarity in the short-range atomic scale structure which essentially affects electronic structures of Fe-B glassy alloys. Such observations have been reported in several amorphous alloys[17].

The peak shift of Fe 3d band with B content shown in Fig. 13 has the trend same to the characteristic concentration dependence found in various physical proerties of Fe-B glassy alloys such as described in INTRODUCTION. The shift of B.E. of 3d band toward lower energy region results in a decrease in the density of states at the Fermi energy E_f. The XPS study for crystalline Fe-Ni alloys by Brendt et al[18] has suggested that the density of states at E_f shows the maximum at the concentration of 40 at%Ni where invar characteristcs occur. Such a behavior was not found in Fe-B glassy alloys with invar proerty.

γ-RAY COMPTON SCATTERING

Based on magnetic measurements the electronic structure of amorphous transition metal-metalloid alloys has been explained in terms of charge transfer from metalloid atom to 3d band holes of transition metals[19]. However, as described in XPS study, a new bonding state is definitely formed between B 2p and Fe 3d electrons in Fe-B glassy alloys. In this study, the measurement of Compton profiles is applied to investigate the electronic structure of Fe-B glassy alloys prepared by melt-spinning.

During last ten years Compton scattering studies have been extensively developed in both the theoretical and experimental fields and established as a powerful technique to obtain directly the information on electronic structures of various kinds of materials[20].

Within the framework of impulse approximation, Compton profile J(q) is directly related to the wavefunction of electrons in specimen, i.e.

$$J(q) = \int_{-\infty}^{\infty}\int \left|\chi(\vec{p})*\chi(\vec{p})\right| dp_x dp_y \quad , \quad (q=p_z) \quad , \qquad (1)$$

where q means the projection of ground state electron momentum $\vec{p}=(p_x,p_y,p_x)$ on the scattering vector and $\chi(\vec{p})$ is the momentum wavefunction defined as Fourier transform of real space wavefunction $\Psi(\vec{r})$ as follows

$$\chi(\vec{p}) = (2\pi)^{-3/2} \int \Psi(\vec{r}) \exp(-i\vec{p}\vec{r}) d\vec{r} \ . \qquad (2)$$

Therefore, we can directly measure the nature of chemical bonding and charge transfer even in disordered materials using Compton scattering.

All the measurements of Compton profiles were carried out using 59.54 keV γ-ray emitted from ^{241}Am radioisotope and a Ge solid state detector. The experimental apparatus used in this study is almost identical to that described in a previous paper[21] except for a sample holder. In the case of the measurement of the Compton profile for boron powder a sample vessel of 5 mm in thickness with mylar windows of 5 μm in thickness was used.

The background correction for mylar windows were made. The multiple scattering correction described elsewhere[21,22] was neglected in this work, because the thickness of the samples was thin enough to avoid the distortion of observed Compton profiles. The deconvolution of an experimental resolution function was applied to raw profiles by generalized least squares method of Fourier analysis[21] using k=3 and λ=300 in eqs. 3-6 in ref.[21]. Details of the performance of the Compton scattering spectrometer and the data processing procedures have been fully descibed in the previous paper[21].

The final Compton profile for each sample was normalized to the normalization value N' which is equal to the area under the theoretical profile calculated from Clementi's free atom wavefunctions[23] over the range of q(a.u.) from -6.0 to +6.0 a.u.

Solid curves in Fig. 14 show experimental Compton profiles J(q) of pure Fe crystal, Fe-15at%B and Fe-18at%B glassy alloys and Fe_2B crysyal, respectively. Dotted lines in Fig. 14 are the theoretical profile for core electrons of which configuration provides the best-fitting to the experimental profile over high momentum region of $q>q_f$(q_f:Fermi momentum) within experimental errors. The theoretical core profile $J^c_{Fe-B}(q)$ as shown by dotted lines in Fig. 14 was calculated as

$$J^c_{Fe-B}(q) = c_{Fe} J^c_{Fe}(q) + c_B J^c_B(q) \ , \qquad (3)$$

where c_{Fe} and c_B are the concentration fraction of Fe and B in the alloys and $J^c_{Fe}(q)$ and $J^c_B(q)$ are the best-fitting core profiles of Fe and B calculated using Clementi's free atom wavefunctions[23].

The core electron configurations of Fe atom thus obtained are summarized as follows

pure Fe crystal	1s(2),2s(2),2p(6),3s(2),3p(6),3d(6.7-7.0)
Fe-15at%B glassy alloy	---------- ,3d(6.5-6.6)
Fe-18at%B glassy alloy	---------- ,3d(6.4-6.8)
Fe_2B crystal	---------- ,3d($\geq$7.0),

while the core electron configuration of B atom is fixed at 1s(2) in the alloys.

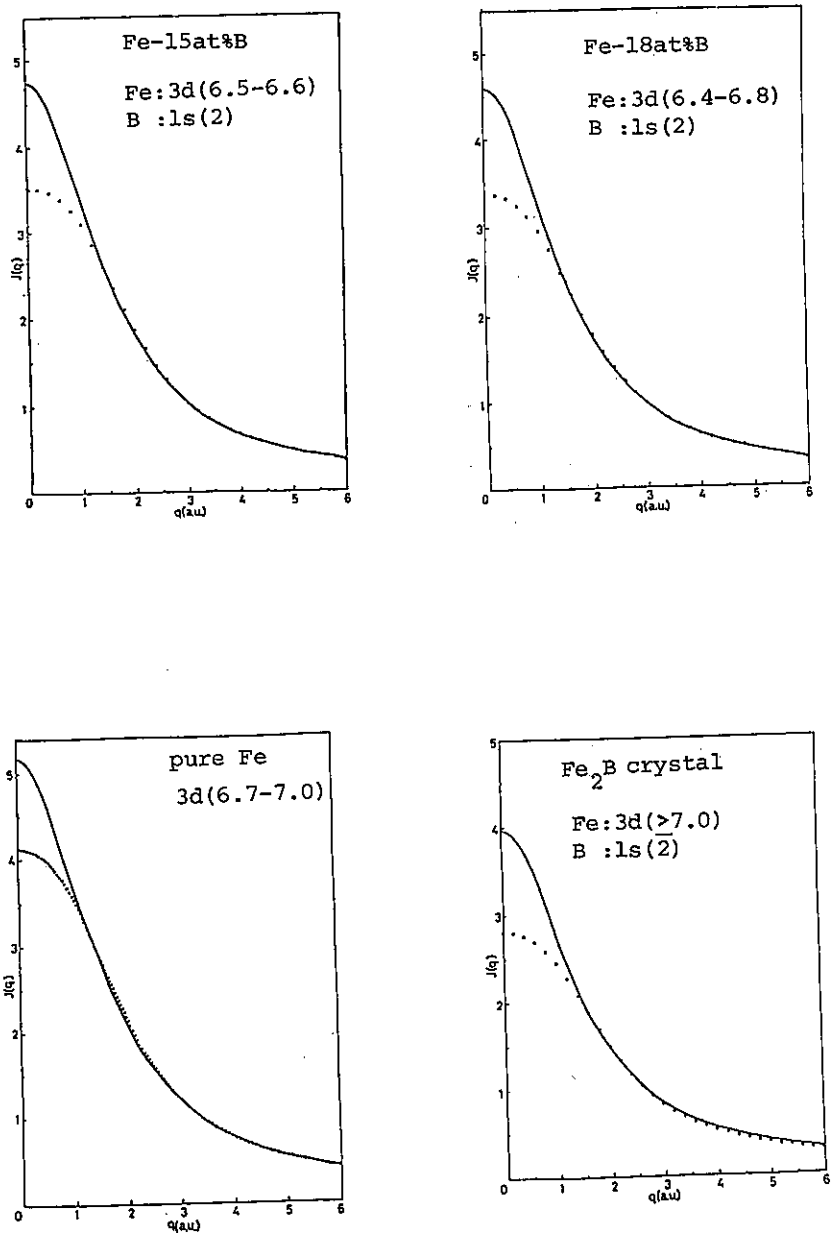

Fig. 14 Experimental Compton profiles J(q)(solid curves) and best-fitting core electron profiles using Clementi's free atom wavefunctions (dotted lines) of pure Fe crystal, Fe-15at%B and Fe-18at%B glassy and Fe_2B crystalline compound.

The present result of the 3d electron configuration 3d(6.7-7.0) in pure Fe crystal is close to the value reported by Paakkari et al[24]. The number of 3d core electrons is decreased in Fe-B glassy alloys compared with that in pure Fe crystal, while Fe_2B crystal has more 3d core electrons than pure Fe crystal. This observation may indicate that the charge transfer model proposed by Yamauchi et al[19] in which electrons move from metalloid atoms to 3d band holes in transition metals is not realistic in Fe-B glassy alloys. In this study, we cannot find a significant difference of the 3d electron number in the core part of Fe atoms between Fe-15at%B and Fe-18at%B glassy alloys.

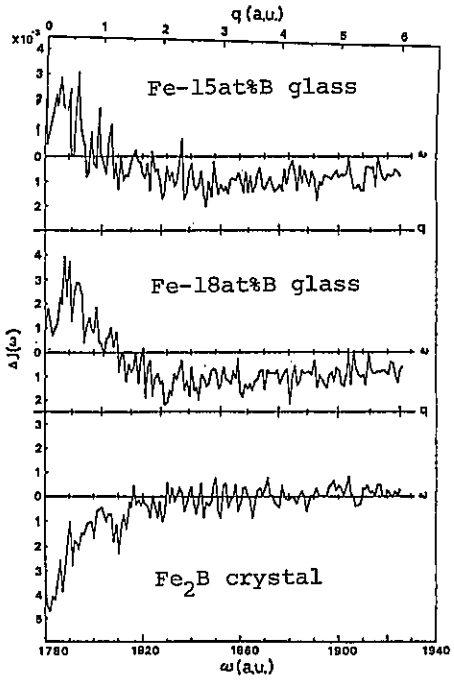

Fig. 15 Differential Compton profiles in energy space $\Delta J(\omega)$ of Fe-B glassy alloys and Fe_2B crystalline compound.

In order to explore more clearly the alloying effect on the electronic structure of Fe-B glassy alloys, we introduce the differential Compton profile $\Delta J(\omega)$ defined as

$$\Delta J(\omega) = J_{Fe-B}(\omega) - \{ c_{Fe} J_{Fe}(\omega) + c_B J_B(\omega) \} , \qquad (4)$$

where $J_{Fe-B}(\omega)$, $J_{Fe}(\omega)$ and $J_B(\omega)$ are raw Compton profiles in energy space for Fe-B alloys, pure Fe crystal and B powder, respectively. The $\Delta J(\omega)$'s for Fe-15at%B and Fe-18at%B glassy alloys and Fe_2B crystal are shown in Fig. 15.

The great featureof Fig. 15 is that $\Delta J(\omega)$'s of Fe-B glassy alloys become positive in low ω region approaching $\omega=0$, but Fe_2B crystal has negative $\Delta J(\omega)$ aroud $\omega=0$. Honda et al[25] have found the negative $\Delta J(\omega)$ or Ni-P and Co-P amorphous alloys prepared by electro-deposition technique,

in which a part of valence electrons are transfered from P atoms to 3d band holes of Ni or Co atoms.

On the other hand, the experimental observation of $\Delta J(\omega)>0$ around $\omega=0$ in this study means that the spatial distribution of electrons becomes more broad by alloying and a resultant chemical bonding must be formed between Fe and B atoms in Fe-B glassy alloys. Currently Itoh et al[16] have observed the positive $\Delta J(q)$ with approaching $q=0$ for $VD_{0.68}$ single crystal, from which the formation of some bonding state between V and D atoms has been concluded.

REFERENCES

[1] See JIM Seminar Textbook(1979) on Applications of Amorphous Metals.
[2] K.Fukamichi, M.Kikuchi, S.Arakawa and T.Masumoto, Solid State Communications, 23(1977)955.
[3] M.Matsuura,Solid State Communucations, 30(1979)231.
[4] T.Fukunaga, M.Misawa, K.Fukamichi, T.Masumoto and K.Suzuki, Rapidly Quenched Metals III(edited bu B.Cantor, The Metals Society, London), 2(1978)325.
[5] Y.Waseda and H.S.Chen, phys. stat. sol. (a), 49(1978)387.
[6] H.Hiroyoshi, K.Fukamichi, M.Kikuchi, A.Hoshi and T.Masumoto, Phys. Letters, 65A(1978)163.
[7] R.Oshima and F.E.Fujita, to be pulished.
[8] H.H.Liebermann, Rapidly Quenched Metals III(edited by B.Cantor, The Metals Society, London), 1(1978)34
[9] T.R.Anthony and H.E.Cline, J. Appl. Phys., 49(1978)829.
[10] T.Ichikawa, phys. stat. sol. (a), 19(1973)707.
[11] J.Logan, phys. stat. sol. (a), 32(1975)361.
[12] N.Cowlam, M.Sakata and H.A.Davies, J. Phys. F, 9(1979)L203.
[13] S.Fujime, Japan. J. Appl. Phys., 5(1966)1029.
[14] K.Terakura and J.Kanamori, Prog. Theor. Phys., 46(1976)1007.
[15] Y.Fukai, S.Kazama, K.Tanaka and M.Matsumoto, Solid. State Communications, 19(1976)507.
[16] F.Itoh, T.Honda, H.Asano, M.Hirabayashi and K.Suzuki, J. Phys. Soc. Jpn., 48(1980) in press.
[17] K.Suzuki, F.Itoh, T.Fukunaga and T.Honda, Rapidly Quenched Metals III (edited by B.Cantor, The Metals Society, London), 2(1978)412.
[18] K.Brendt, U.Marx and O.Brummer, phys. stat. sol. (b), 90(1978)487.
[19] K.Yamauchi and T.Mizoguchi, J. Phys. Soc. Japan, 39(1975)541.
[20] K.Suzuki and F.Itoh, Progress in the Study of Applications of Electron Theory to Materials Science(ed. M.Doyama, Univ. Tokyo, 1978)p.258.
[21] F.Itoh, T.Honda and K.Suzuki, J. Phys. Soc. Jpn., 47(1979)122.
[22] F.Itoh, T.Honda and K.Suzuki, J. Phys. Soc. Jpn., 46(1979)1201.
[23] E.Clementi, IBM J. Res. Dev. Suppl., 9(1965)2.
[24] T.Paakkari, S.Manninen and K.F.Berggren, Phys. Fenn., 10(1975)207.
[25] T.Honda, F.Itoh, T.Fukunaga and K.Suzuki, Sci. Rep. RITU A(1980) in press.